

# Two New Catalogues of Superclusters of Abell/ACO Galaxy Clusters out to redshift 0.15

M. Chow-Martínez<sup>1</sup> \*, H. Andernach<sup>1</sup>, C. A. Caretta<sup>1</sup>, J. J. Trejo-Alonso<sup>1</sup>

*Departamento de Astronomía, DCNE, Universidad de Guanajuato, Apdo. Postal 144, CP 36000, Guanajuato, Gto., Mexico.*

Accepted . Received ; in original form

## ABSTRACT

We present two new catalogues of superclusters of galaxies out to a redshift of  $z = 0.15$ , based on the Abell/ACO cluster redshift compilation maintained by one of us (HA). The first of these catalogues, the all-sky Main SuperCluster Catalogue (MSCC), is based on only the rich (A-) Abell clusters, and the second one, the Southern SuperCluster Catalogue (SSCC), covers declinations  $\delta < -17^\circ$  and includes the supplementary Abell S-clusters. A tunable Friends-of-Friends (FoF) algorithm was used to account for the cluster density decreasing with redshift and for different selection functions in distinct areas of the sky. We present the full list of Abell clusters used, together with their redshifts and supercluster memberships and including the isolated clusters. The SSCC contains about twice the number of superclusters than MSCC for  $\delta < -17^\circ$ , which we found to be due to: (1) new superclusters formed by A-clusters in their cores and surrounded by S-clusters (50%), (2) new superclusters formed by S-clusters only (40%), (3) redistribution of member clusters by fragmentation of rich (multiplicity  $m > 15$ ) superclusters (8%), and (4) new superclusters formed by the connection of A-clusters through bridges of S-clusters (2%). Power-law fits to the cumulative supercluster multiplicity function yield slopes of  $\alpha = -2.0$  and  $\alpha = -1.9$  for MSCC and SSCC respectively. This power-law behavior is in agreement with the findings for other observational samples of superclusters, but not with that of catalogues based on cosmological simulations.

**Key words:** large-scale structure of Universe - galaxies: clusters: general - cosmology: observations

## 1 INTRODUCTION

Superclusters are usually defined as “clusters of clusters” given that mainly catalogues of galaxy clusters have been used to identify them. De Vaucouleurs (1953) was the first to present evidence of the existence of a large-scale superstructure now known as the Local Supercluster. The superclustering as a general phenomenon was originally advocated by various authors, beginning with Abell (1961), and followed by Bogart & Wagoner (1973), Hauser & Peebles (1973), and Peebles (1974). Taking this definition of superclusters as aggregates of two or more galaxy clusters (e.g. Bahcall & Soneira 1984), supercluster catalogues have been produced using the pseudo-3D distribution of Abell/ACO clusters (Abell 1958; Abell, Corwin & Olowin 1989) by Rood (1976), Thuan (1980), Bahcall & Soneira (1984), Batuski & Burns (1985), West (1989), Zucca et al. (1993), Kalinkov & Kuneva (1995), and Einasto et al. (1994, 1997,

2001), among others. Zucca et al. (1993) were the first to use the total sample of Abell/ACO A-clusters to construct an all-sky catalogue of 69 superclusters within a redshift of  $z \sim 0.1$ , with an overdensity of at least twice the average density, and with at least three member clusters. Einasto et al. (2001) used 1663 A-clusters (64% of them with measured spectroscopic redshifts), out to  $z = 0.13$ , to obtain a catalogue of 285 superclusters via a percolation analysis based on a linking length of  $34 h_{70}^{-1}$  Mpc, assumed constant throughout the considered volume. The number of member clusters (commonly called multiplicity,  $m$ ) ranged from 2 to 35. In addition, they also presented the first catalogue of 19 superclusters based on X-ray luminous clusters detected in the ROSAT All-Sky Survey (Voges et al. 1999). Recently Chon et al. (2013) published a catalogue of 195 superclusters based on the ROSAT-ESO Flux Limited X-Ray Galaxy Cluster Survey (REFLEX II). Some authors have also used catalogues of individual galaxies based on large-scale surveys to search for superclusters, defining these as significant density enhancement of galaxies (e.g. Gregory & Thompson

\* E-mail:marcel@astro.ugto.mx

1978; Giovanelli & Haynes 1993; Quintana et al. 1995; Barmby & Huchra 1998; Hanski et al. 2001; Einasto et al. 2007a, 2011a).

Generally superclusters, being immersed in the “cosmic web”, exhibit irregular or filamentary shapes connected through bridges of galaxies and separated by extensive “void” regions where almost no galaxies are found. Properties of the large-scale structure (determined using both observational data and N-body cosmological simulations) have been discussed, e.g. by Jaaniste et al. (1998), Gramann & Suhhonenko (2002), Kolokotronis et al. (2002), Wray et al. (2006), Einasto et al. (2007b,c,d, 2011b), Costa-Duarte et al. (2011), Luparello et al. (2011), Sousbie (2011), and Sousbie et al. (2011).

Currently there is no evidence that superclusters have reached virialization, since the sizes of these structures range from a few Mpc to  $\sim 150 h_{70}^{-1}$  Mpc, and the crossing time for a member cluster within the system exceeds the age of the Universe (e.g. Oort 1983; Gramann & Suhhonenko 2002). This implies that these systems still preserve a memory of their dynamical history, which makes them worth studying. Furthermore, since they constitute the environment of a considerable fraction of the clusters, groups and galaxies themselves, by comparing their properties with those in lower-density environments we can study the effect of this environment on the evolution of such systems. Galaxy clusters are the most massive systems in the Universe that have condensed out of the Hubble flow, and their evolution is still a matter of vital discussion. Finally, superclusters represent regions of significant density enhancement which cause distortions in the local gravitational field that are sometimes noticeable via the bulk motions towards them (e.g. the case of the Great Attractor, Lynden-Bell et al. 1988). They also provide information on the mass distribution in intercluster space, e.g. by measuring their imprint on the CMB via the Sunyaev-Zeldovich effect (e.g. Planck Collaboration 2013). All these features allow one to constrain and refine cosmological models of the Universe.

In the present work we describe two new catalogues of superclusters based on the update of late 2012 of the Abell/ACO cluster redshift compilation by one of us (for a description of its content cf. Andernach et al. 2005), restricting ourselves to clusters with redshift  $z \leq 0.15$ . For the first catalogue we consider the distribution of Abell/ACO A-clusters (rich clusters) all over the sky, while the second one is a southern sky catalogue ( $\delta < -17^\circ$ ) based on both A-clusters and the supplementary S-clusters (typically poorer than the A-clusters). For the construction of both catalogues we tuned the linking length as a function of redshift and position on the sky, thus allowing for both undersampling at higher redshifts and deeper redshift observations over certain areas of the sky, like those covered by the Sloan Digital Sky Survey (Abazajian et al. 2009). The effect of the inclusion of the S-clusters in the large-scale structure is studied by comparing the two catalogues. We also discuss the cumulative distribution of multiplicities (number of member clusters) for the superclusters in the Local Universe, based on both observational and simulated data.

The paper is organized as follows. In section 2 we describe our Abell/ACO cluster sample; in section 3 we discuss and explain the percolation analysis we applied; section 4 explains the generated catalogues and compares them with

that of Einasto et al. (2001); in section 5 we present some properties of the large-scale structure by intercomparing our catalogues, and by comparing their multiplicity functions with the ones obtained for different supercluster samples, including supercluster catalogues generated from distributions of equivalent dark matter haloes in cosmological simulations. Section 6 presents our conclusions and summary.

Throughout this paper we assume the following cosmological parameters:  $H_0 = 70 h_{70} \text{ km s}^{-1} \text{ Mpc}^{-1}$ ,  $\Omega_M = 0.3$ , and  $\Omega_\Lambda = 0.7$ .

## 2 DATA

The Abell/ACO cluster redshift compilation used here (e.g. Andernach et al. 2005) is a collection of individual radial velocities for potential member galaxies of such clusters. The compilation has been updated since 1989 (Andernach 1991; Andernach et al. 1995; Andernach & Tago 1998) by monitoring redshift data of galaxies from the published literature and a few unpublished references. The compilation, as of late 2012, contains redshifts for about 130,000 individual cluster galaxies in 3930 different Abell clusters. Whenever a cluster shows more than one concentration along the line of sight, separated in redshift by more than  $\sim 1500 \text{ km s}^{-1}$ , we register these as components A, B, C,... in increasing order of redshift. In many cases, the component with the dominant number of redshifts is clearly the one recognized by Abell/ACO, while in other cases these components may be similarly populated, and the identification is not straightforward. In what follows, we shall refer to these as *line-of-sight components* of a cluster, and we include all the detected ones in our analysis out to  $z = 0.15$ .

With the advent of large-scale multi-object spectroscopic surveys, like the Two-Degree Field Galaxy Redshift Survey (2dFGRS, Colles et al. 2001), the Six-Degree Field Galaxy Redshift Survey (6dFGRS, Jones et al. 2004), and the Sloan Digital Sky Survey (e.g. SDSS-DR7, Abazajian et al. 2009), the source of redshifts for this compilation has gradually changed from surveys of individual clusters to large-area redshifts surveys, resulting in more redshifts for cluster members from fewer references per year. We include a number of new spectroscopic redshifts obtained by us for galaxies in 121 clusters. These will be published in a separate paper. Furthermore, for clusters with no spectroscopic redshift as yet, the compilation also includes estimated redshifts, kindly provided by M. West (2007, private communication) and based on the relation proposed by Peacock & West (1992).

The current compilation includes all 4076 A- and 1174 S-clusters. For 1011 of the A-clusters we list a total of 2511 line-of-sight components, resulting in altogether 5576 clusters/components, while 230 S-clusters are split into 551 components, resulting in a total of 1495 S-clusters/components. From these we selected the ones with redshift below 0.15 as the basis for our search for superclusters. These were 3410 A-clusters/components (92% of them having measured spectroscopic redshifts for at least one member, and 76% for at least three galaxies), and 1168 S-clusters/components (91% with at least one galaxy with measured spectroscopic redshift, and 69% with at least three). Beyond this redshift the sample becomes noticeably more incomplete. The redshift

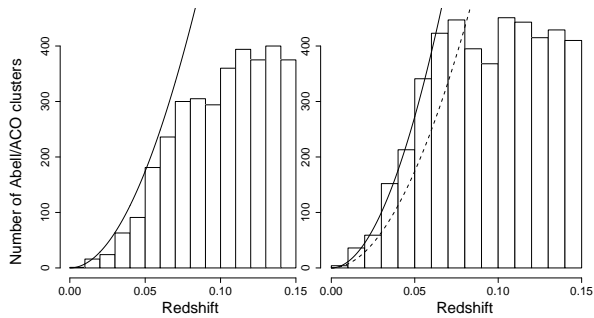


**Figure 1.** Redshift distribution for the A-clusters (left panel) and A+S clusters (right panel). The solid lines are the expected number of clusters in spherical shells of  $\Delta z = 0.01$  using a constant space density of clusters corresponding to the most completely surveyed redshifts for each distribution, namely  $0.03 < z < 0.07$  for the all-sky distribution of A-clusters, and  $z < 0.05$  for the A+S clusters in the southern ( $\delta < -17^\circ$ ) sample. These values are:  $7.4 \times 10^{-6} h_{70}^3 \text{ Mpc}^{-3}$  for only the A-clusters and  $2.8 \times 10^{-5} h_{70}^3 \text{ Mpc}^{-3}$  for A- and S-clusters together in the south. The first value is comparable to the one found by Einasto et al. (1997) ( $8.9 \times 10^{-6} h_{70}^3 \text{ Mpc}^{-3}$ ) for Abell/ACO clusters. The dashed line in the right panel indicates the same function as the solid line in the left panel. These curves grow according to  $r^2$  where  $r = r(z)$  is the comoving distance as described by Hogg (2000).

distribution for both samples is shown in Figure 1. The S-clusters represent an important contribution in the southern sky, and they complement the sample toward lower richness clusters in this region at lower redshifts.

In Figure 2 we divided the entire sample in subsamples according to their position on the sky, in order to identify systematic effects in their global distribution. In the northern sample the main effect is the presence of the SDSS redshift data: where these data exist the clusters are more completely spectroscopically sampled such that more clusters enter in the sample at relatively high redshifts ( $z \gtrsim 0.06$ ). On the other hand, the S-clusters affect the southern sample especially at lower redshifts ( $z \lesssim 0.08$ ) such that the first peak in redshift in the second panel of both Figs. 1 and 2 is dominated by them. In the redshift range considered here, the S-clusters are almost exclusively poorer systems than the A-clusters. Thus, we decided to divide our sample into four, rather than two, subsamples, namely two northern subsamples, one for the SDSS region and another for the rest of the northern sky, and another two southern subsamples ( $\delta < -17^\circ$ ), one including both A- and S-clusters and the other only the A-clusters.

### 3 PERCOLATION ANALYSIS

The Friends-of-Friends algorithm (FoF, e.g. Turner et al. 1976; Zel'dovich et al. 1982; Huchra & Geller 1982; Einasto et al. 1984) is frequently used to link points when we do not know *a priori* how they are distributed. In a virialized regime, such as we expect for at least the cores of the galaxy clusters, the linking length is determined by assuming a spherical gravitational collapse model (e.g. Caretta et al. 2008). However, since the superclusters are probably not in an equilibrium state, we can not derive the ideal linking length in this way.

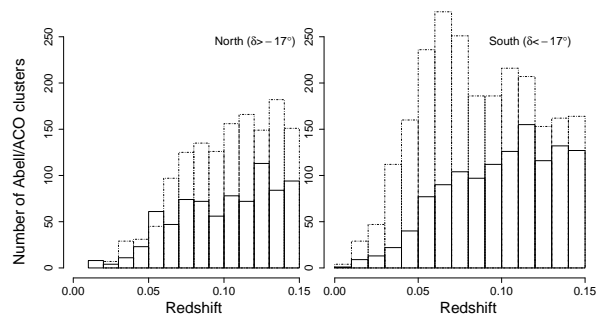


**Figure 2.** Redshift distribution for the northern and southern Abell/ACO clusters. For the northern subsample, the solid histogram is for the northern sky without the SDSS region and the dashed histogram is the one for the SDSS region. For the southern subsample, the solid histogram is the distribution for A clusters and the dashed histogram is the one for A+S clusters.

In the percolation analysis, the method usually used for identifying superclusters of galaxies, the linking length of the FoF is chosen such that it maximizes the number of systems formed. The result of the percolation analysis depends strongly on the linking length ( $\ell$ ). For smaller linking lengths the FoF yields a smaller number of only the densest systems, while for larger linking lengths these systems start to connect among themselves, lowering the total number of systems until a complete percolation of the sample is reached (e.g. Einasto et al. 1984). For this reason, in the identification of superclusters of galaxies, the linking length of the FoF is often chosen such that it maximizes the number of systems formed in the percolation process. We shall call this the *critical linking length*,  $\ell_c$ . The percolation analysis relies on the fact that the mean density is correctly represented (i.e. the completeness of the sample) in the considered volume. In an ideal (complete and homogeneous) sample, the critical linking length obtained this way should be the same throughout the entire volume. Since the distribution of the clusters in our sample is clearly less complete at higher redshifts (see Figures 1 and 2), and also differs from one subsample to the other, the choice of a single critical linking length for a supercluster search based on Abell/ACO clusters is certainly not the best solution. Therefore, we used a *tunable* value of  $\ell_c$ , which is allowed to vary with the selection function and thus corrects for completeness variations in both redshift and position on the sky. This selection function (the fraction of clusters missed as a function of the redshift, due to an inhomogeneous sampling and the Malmquist bias) is measured directly by estimating the value of  $\ell_c$  in the four different subsamples and in different redshift ranges.

To this end we divided each subsample into seven spherical shells with a width of  $\Delta z = 0.03$ , (allowing an overlap between them of  $\delta z = 0.01$ ), inside which the density is not expected to vary significantly. Thus, the first bin ranges from  $z = 0.00$  to  $z = 0.03$ , the second one from  $z = 0.02$  to  $z = 0.05$ , and so on. We obtained the value of  $\ell_c$  for each redshift “shell” and constructed the so-called “Percolation Function” (PF), i.e. the value of  $\ell_c$  as function of the redshift. Percolation functions for each subsample are shown in Figure 3. Three different PF were chosen. The first of these is the combination of the northern sample (excluding the SDSS region) and the southern sample (excluding the S-

clusters), which we call the *Master PF*. As expected, these two subsamples show a similar behavior. The second PF is that for the SDSS region, which we call the *SDSS PF*. Since it is poorly sampled at lower redshifts ( $z < 0.06$ ), we first freely fitted the data and, then, forced it to coincide with the Master PF at  $z = 0.06$ , taking the Master PF as the SDSS PF for redshifts lower than this. The third PF is that for the southern subsample including the S-clusters, which we call the *Southern PF*. This latter one presents smaller critical linking lengths,  $\ell_c$  than the Master PF at every redshift, and especially so at the lowest redshifts, obviously due to the higher space density of clusters when S-clusters are included.

The redshift range in which the PFs reach their lowest value may be interpreted as the one of highest completeness, and *vice-versa*: in an undersampled region, the value of  $\ell_c$  is larger. Thus, employing these PFs in our FoF compensates for the loss of objects due to selection effects. According to these curves, the best sampled region (excluding the contribution of SDSS and S-clusters) is near  $z \sim 0.06$ , where the Master PF reaches its minimum. At lower redshifts the sample suffers a deficiency due to the exclusion of clusters at  $z \leq 0.02$ , as imposed by the authors of the Abell/ACO catalogues. At higher redshifts the undersampling is due to limiting sensitivity of the sky surveys used to find the clusters and incompleteness in the spectroscopic sampling. The SDSS PF has smaller values than the Master PF at higher redshifts due to the more complete sampling of the SDSS. As a consequence of the inclusion of the S-clusters, the Southern PF is always smaller than the Master PF, especially at lower redshifts. Near the minimum of the Master PF (i.e. where the sampling is best, near  $z = 0.06$ ) we find  $\ell_c \sim 23 h_{70}^{-1}$  Mpc while for lower redshifts the Southern PF reaches a minimum that corresponds to a  $\ell_c \sim 12 h_{70}^{-1}$  Mpc.

## 4 SUPERCLUSTERS OF ABELL/ACO GALAXY CLUSTERS

### 4.1 The Catalogues

The Master and SDSS PFs were used to produce the *Main SuperCluster Catalogue* (MSCC) based on the all-sky sample of A-clusters. The MSCC contains 601 superclusters with multiplicities between 2 and 42. The *Southern SuperCluster Catalogue* (SSCC) was produced using the Southern PF, and contains 423 superclusters with multiplicities between 2 and 38. For the rest of this paper we shall refer to individual superclusters with their MSCC and SSCC acronyms, followed by their sequence number (see Tables 1 and 2).

For the MSCC, 1152 clusters (34% of the total number of clusters) turn out to be isolated, while this number is 870 (36%) for the SSCC. The fractions of superclusters with multiplicity  $m = 2$  (pairs of clusters) are 48% and 52% (containing 17% and 19% of the input clusters), in the MSCC and SSCC, respectively. The richest superclusters, with  $m > 10$ , represent 4% in both MSCC and SSCC, whose member clusters constitute 49%, and 45% of the input clusters for MSCC and SSCC, respectively. We also flagged as *supercluster candidates* the ones which would not be found by our FoF in a test catalogue that excludes the clusters with estimated redshifts. In our Abell/ACO sample limited to  $z \leq 0.15$ ,

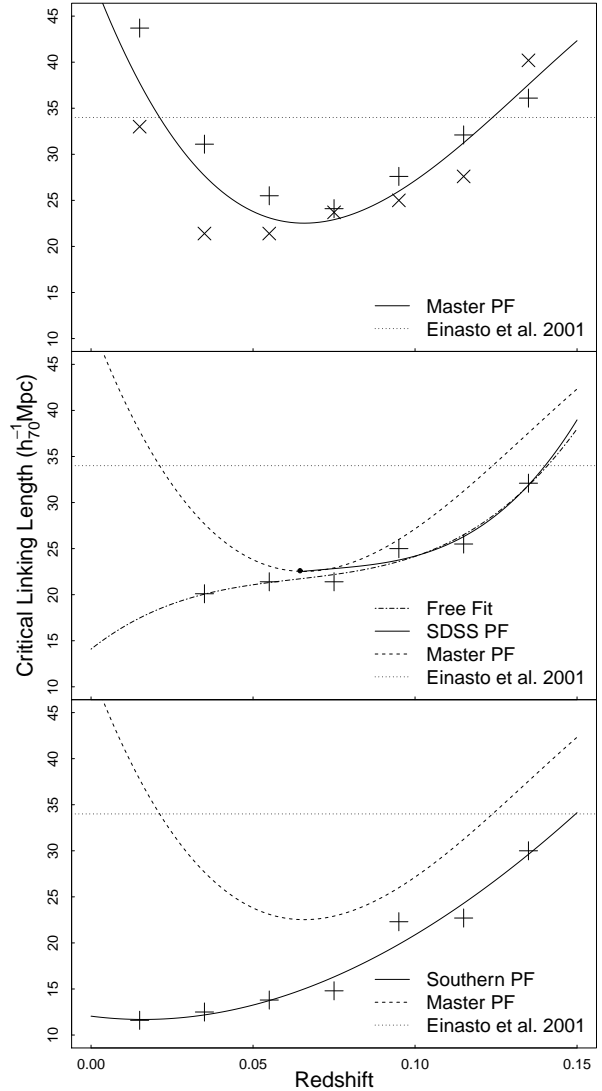


**Figure 3.** Percolation functions (PFs) for the considered samples. Top panel: PF for the Northern region (excluding the SDSS) and the Southern region (excluding S-clusters), the former marked with “+” signs and the latter one with “x” signs; the fit is what we call the *Master PF*. Middle panel: PF for the SDSS region, the dashed line is the Master PF, the dot-dashed line is a free fitting for the SDSS region, and the solid line is the curve we call the *SDSS PF*, in which the SDSS PF is forced to follow the Master PF for  $z \leq 0.06$ . Bottom panel: PF for the complete southern sample (including S-clusters), where the Master PF is again represented by the dashed line and the Southern PF by the solid line. For comparison, the linking length used by Einasto et al. 2001 is indicated with a dotted line.

out of 4578 clusters (including A- and S-clusters as well as their line-of-sight components) there are 358 with only estimated redshifts, identified with an “e” following their names in Tables 1 and 2. Using the above definition, 37 (6%) of the MSCC and 38 (9%) of the SSCC superclusters are candidates, identified in the catalogues with a letter “c” following the supercluster sequence number.

We also include in Tables 1 and 2 the supercluster ID of Einasto et al. (2001) for some specific cases (187 for

**Table 1.** First ten entries in MSCC: (1) MSCC number; (2) SCL identification; (3) multiplicity,  $m$ ; (4,5) right ascension and declination (J2000) in decimal degrees; (6) redshift,  $z$ ; (7) distance, in  $h_{70}^{-1}$  Mpc, of the pair of clusters with the maximum separation in each supercluster; (8) list of member clusters of the supercluster. The full table is available online.

MSCC	SCL	$m$	$RA_J$	$Dec_J$	$z_{SC}$	$d_{\max}$	Abell/ACO member clusters
1	–	9	0.77	–26.72	0.064	50.6	A0014, A0020, A2683A, A2716, A2726A, A2734, A4038C, A4049B, A4053B
2	3	2	1.09	+09.77	0.098	20.2	A2694, A2706
3	–	4	1.20	+16.05	0.119	41.5	A0001, A2688A, A2703, A2705
4	3	4	1.26	+02.89	0.098	33.4	A0003, A2696B, A2698, A2700A
5	–	2	1.31	–15.32	0.102	20.3	A2699, A2710A
6	–	4	1.58	–64.24	0.116	37.7	A2732, A2740A, A2760, A4028
7	220	3	2.03	–36.93	0.049	28.5	A2717A, A2771A, A4059
8	5,9	10	2.09	–35.26	0.117	79.4	A2715B, A2721A, A2721B, A2724, A2730, A2749B, A2767, A2772, A4035A, A4074A
9	–	2	2.35	–10.57	0.110	16.2	A0008A, A2709B
10	–	3	3.06	–34.91	0.096	22.4	A2715A, A2749A, A2755

**Table 2.** First ten entries in SSCC: (1) SSCC number; (2) SCL identification; (3) multiplicity,  $m$ ; (4,5) right ascension and declination (J2000) in decimal degrees; (6) redshift,  $z$ ; (7) distance, in  $h_{70}^{-1}$  Mpc, of the pair of clusters with the maximum separation in each supercluster; (8) list of member clusters of the supercluster. The full table is available online.

SSCC	SCL	$m$	$RA_J$	$Dec_J$	$z_{SC}$	$d_{\max}$	Abell/ACO member clusters
1	–	2	0.20	–23.73	0.097	18.8	A2681, A2719
2	5	11	0.68	–34.92	0.116	80.0	A2715B, A2721A, A2721B, A2730, A2749B, A4035A, A4074A, S0012B, S1161C, S1161D, S1170B
3	–	2	0.80	–44.78	0.038	10.9	S0005, S1173
4	–	3	1.23	–38.67	0.103	24.2	A4068, S0017e, S1172C
5	–	2	2.61	–30.93	0.070	14.0	A2751A, S0006D
6	–	2	3.38	–29.83	0.123	24.7	A2759B, S0010
7c	–	2	3.91	–65.43	0.148	24.2	A2737e, A2761e
8	–	5	4.23	–64.81	0.114	31.7	A2732, A2740A, A2760, S0018e, S0057e
9	–	2	4.24	–35.03	0.095	4.2	A2749A, A2755
10	–	2	4.34	–23.26	0.066	11.8	A0014, A0020

MSCC and 117 for SSCC) where a certain minimum fraction of member clusters (explained below) in that catalogue is linked to the respective supercluster here. From now on, we shall denote Einasto et al. (2001) superclusters ID with the prefix SCL, as chosen by these authors. Tables 1 and 2 only include the cross-identifications when the association was sufficiently clear, with minimum ambiguities by fragmentations or “noise” from subcomponents (divisions of the superclusters due to their member clusters having line-of-sight components). We assumed an entry in SCL to be the same as one in MSCC/SSCC when the number of coincident member clusters exceeded a certain fraction or when the main member cluster of well-known superclusters (e.g. those listed in Section 4.3) was found to be the same. The minimum fraction of member clusters required for the match depended on the multiplicity in MSCC: for pairs, we required both clusters to coincide; for triple and quadruple systems we required at least two equal member clusters. For higher multiplicities ( $m \geq 5$ ) we accepted “fragments” (i.e. a subsample of member clusters) of the original superclusters listed in SCL, and, as we said, in some cases we allowed fractions lower than 50% when the main member clusters were present in some particular MSCC. Where more than one entry in SCL match the same MSCC/SSCC, all SCL ID of these contributors are included (e.g. MSCC 8 in Table 1), in order of decreasing fraction of coincident member clusters

(cases for which only one coincident cluster was found are not listed). For SSCC, as we will discuss in Section 5.1, this fragmentation is stronger, so we accepted an identification with SCL when we had at least two coincidences of original member clusters for the fragments of richest superclusters. This was done because fragments usually are accompanied by S-clusters in SSCC. In Section 4.2 we explain this matching procedure in more detail, including our treatment of clusters with line-of-sight components. There we also present more complete statistics accounting for more complex cases.

The MSCC and SSCC catalogues (Tables 1 and 2) contain the following columns: (1) the supercluster ID in the respective catalogue followed by the letter “c” if the supercluster is considered a candidate; (2) the matching SCL from Einasto et al. (2001) where applicable; two or more, at most four, SCL ID’s appear if we found these SCL’s identifiable with the same MSCC or SSCC; (3) the multiplicity  $m$ , i.e. the number of member clusters; (4) right ascension and (5) declination (for equinox J2000, in decimal degrees), obtained as the simple arithmetic mean of the member cluster positions; (6) the arithmetic mean redshift  $z_{SC}$  of the member clusters, including clusters with estimated redshift; (7) the 3D-distance between the most separate pair of member clusters in each supercluster, in  $h_{70}^{-1}$  Mpc, as an estimation of the supercluster size; (8) the list of the member clusters,

appended by an “e” if that cluster had only an estimated redshift. Letters A, B, C, ... appended to the cluster name indicate a line-of-sight component in order of increasing redshift.

Table 3 lists all clusters used in our analysis, both isolated ones and supercluster members, including all line-of-sight components within the considered volume of  $z \leq 0.15$ . Again, where the name of the cluster is followed by the flag “e” in the first column of Table 3, the listed redshift is estimated. The third and fourth columns indicate the membership in MSCC or SSCC, where isolated clusters are marked with “iso”. For line-of-sight components of clusters (labelled A, B, ..., etc.), we list the percentage of galaxies with measured redshift that contribute to the line-of-sight component. Since not all line-of-sight components are inside the examined volume ( $z \leq 0.15$ ), in a few cases the sum of the fraction is lower than 100%.

The projected sky distributions of both catalogues are displayed in Figure 4.

#### 4.2 Comparison with Previous Supercluster Catalogues

A comparison of the MSCC and SCL catalogues should give an idea of the improvements achieved over the last 15 years, mainly due to (a) the inclusion of new redshifts from the recent literature, (b) the extension to a higher redshift limit, and (c) the inclusion of all redshift components for the individual clusters, when they are present. Einasto et al. (2001) found 285 superclusters based on a critical linking length of  $\ell_c = 34 h_{70}^{-1}$  Mpc, assumed to be constant throughout the considered volume out to  $z_{lim} = 0.13$ . Rather than all line-of-sight components, these authors used only the component with the largest number of spectroscopic redshifts, assuming this one to be the “correct” Abell/ACO cluster. The cluster sample used by Einasto et al. (2001) consisted of 1663 A-clusters, 64% of which had measured redshifts. Of these, 1163 clusters (70%) were found to be members of pairs or superclusters, about 5% more than what we found for MSCC and SSCC.

To compare our MSCC with the SCL catalogue we performed a cluster-by-cluster cross-matching. In the case of clusters with line-of-sight components, only the dominant component was taken into account for the comparison, defining this as the component with the largest number of spectroscopically measured galaxies (in an attempt to match the definition used by Einasto et al. 2001).

Based on the above, of the total number of clusters (1159) which are members of any of the 285 “SCL” superclusters, 880 (76%) were located within 356 superclusters of MSCC, while another 279 (24%) were found to be isolated in MSCC. Moreover, the remaining 245 MSCC superclusters, which are new compared to SCL, can be divided into: 112 (46%) which are beyond the redshift limit of SCL ( $z_{lim} = 0.13$ ) and another 14 (6%) which are close to that limit, such that they have members on both sides of that limit; another 47 (19%) resulted to be actually “components” in the line of sight of superclusters, formed mostly by part of the members of the “dominant” supercluster; 35 (14%) are superclusters comprised by line-of-sight components accompanying clusters that were considered isolated in SCL; and finally, 37 (15%) represent completely new su-

**Table 3.** The first ten entries of the list of clusters used as input catalogue for MSCC and SSCC. Columns are: (1) Abell/ACO number/ID (including all line-of-sight components within  $z \leq 0.15$ ); (2) measured or estimated redshift; (3) and (4) sequence number of the respective MSCC and SSCC supercluster host, or “iso” if the cluster is isolated in the respective catalogue, a “—” indicates that the cluster was not used in the respective input catalogue (northern clusters for SSCC and S-clusters for MSCC); (5) in case of line-of-sight components, percentage of galaxies with measured redshift in each component is listed. The full table is available online.

Abell/ACO	$z$	MSCC	SSCC	%
A0001	0.1249	3	—	—
A0002	0.1225	iso	iso	—
A0003	0.1022	4	—	—
A0005e	0.1120	iso	—	—
A0007	0.1030	iso	—	—
A0008A	0.1092	9	—	62
A0008B	0.1441	iso	—	38
A0012	0.1259	iso	—	—
A0013	0.0946	iso	iso	—
A0014	0.0653	1	10	—

perclusters within the volume considered by Einasto et al. (2001)<sup>1</sup>.

Of the 255 superclusters of SCL whose clusters have a match in some MSCC supercluster, 108 (42%) had a one-to-one match in MSCC, while 106 (42%) were “fragmented” (member clusters were linked into different superclusters in MSCC). Another 41 (16%) SCL were redistributed in more complex ways; their member clusters are part of one unique MSCC supercluster which also have member clusters of one or more other SCL superclusters. This implies that, in some cases for example, the members of three SCL are redistributed in two MSCC. The statistics of the components, fraction of measured redshift and fraction of isolated clusters for the SCL, MSCC, and SSCC catalogues, are listed in Table 4.

A total of 114 (40%) superclusters in SCL were labelled as candidates (“c”). Only for the sake of comparison, when we use the same criterion for “candidate” as Einasto et al. (2001), we find that 81 candidates in SCL are in fact not superclusters in MSCC (i.e. their members were not linked). Another two SCL superclusters were partially confirmed, i.e., they appear fragmented as two MSCC superclusters, one of them being still a candidate. Another 21 candidates in SCL are confirmed in MSCC, and a further 10 superclusters appear as candidates in both MSCC and SCL. In MSCC there are 37 (6%) supercluster candidates (according to our definition), of which 25 are new superclusters, with 22 of these 25 exceeding the limit  $z_{lim} = 0.13$  imposed by Einasto et al. (2001).

#### 4.3 Notes on Individual Superclusters

We searched the literature for previous studies of the richest superclusters in MSCC and SSCC (i.e. those 13 MSCC and

<sup>1</sup> One of these cases is the pair MSCC 164, formed by the clusters A0569N and A0569S (e.g. Beers et al. 1991).

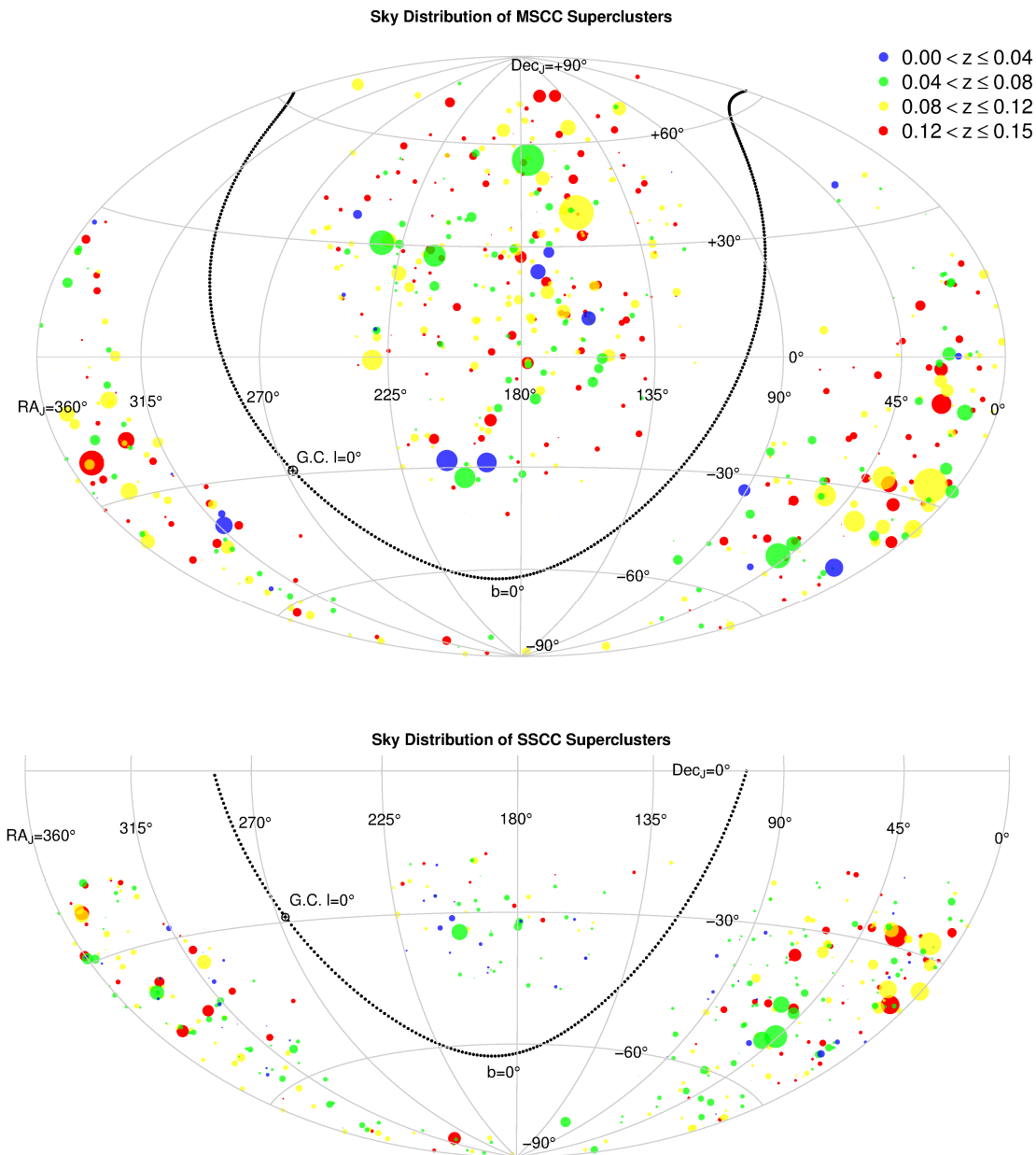


**Figure 4.** Sky distribution in an Aitoff projection of equatorial coordinates of superclusters in MSCC (top panel), and SSCC (bottom panel). The superclusters are colored according to their location in four redshift intervals (see legend at top right). The symbol size is proportional to the separation  $d_{\max}$ , of member cluster pairs in each supercluster (cf. Table 1), and the ratio of symbol size to  $d_{\max}$  decreases slightly with increasing redshift interval. In both projections the black dotted line indicates the Galactic plane ( $b = 0^\circ$ ) and “G.C.” denotes the Galactic centre.

11 SSCC with  $m \geq 14$ ) in order to explore the reliability of these catalogues. Only one of these richest superclusters, SSCC 82, which exceeds  $z = 0.13$ , had not been identified before. This comparison also gave some clues on the differences between MSCC and SSCC caused by the inclusion of S-clusters in SSCC.

**Sculptor (SCL009):** Identified as MSCC 33 and SSCC 36, with similar multiplicities (24 and 22, respectively), although more compact in the SSCC where 9 A-

clusters were not linked while another five S-clusters entered the supercluster. These S-clusters connect the main structure of MSCC 33 with the pair MSCC 47. The main member clusters, A2798, A2801, A2804, A2811, and A2814, studied before by Obayashi et al. (1998) and more recently by Sato et al. (2010), remain in both catalogues as the possible “core” of *Sculptor*.

**Pisces-Cetus (SCL010):** Is one of the 4 richest superclusters in SCL (together with Shapley, *Sculptor*, and *Aquarius*); fragmented in 3 structures in our anali-

**Table 4.** Brief comparison between SCL, MSCC, and SSCC. Columns are: (1) catalogue acronym; (2) and (3) number of A/S clusters not considering line-of-sight components; (4) and (5) total number of A/S clusters including line-of-sight components; (6) and (7) fraction of A/S clusters with spectroscopic redshift in each catalogue not considering line-of-sight components (including line-of-sight components); and (8,9,10) fraction of input clusters that resulted to be isolated, members of pairs and members of supercluster ( $m \geq 3$ ) systems.

	Clusters		Components		Fraction of $z_{spec}$		Fraction of clusters that are		
	A	S	A	S	A	S	Isolated	in Pairs	in Superclusters
SCL	1663	–	–	–	64.4%	–	30.1%	15.5%	54.4%
MSCC	2531	–	3410	–	90.0 (92.6)%	–	33.8%	17.1%	49.1%
SSCC	974	869	1217	1168	87.4 (89.9)%	88.0 (91.1)%	36.5%	18.7%	44.8%

sis: MSCC 39, the northern *Pisces-Cetus* (with  $m = 11$ ); MSCC 27, the central *Pisces-Cetus* ( $m = 9$ ); and MSCC 1, the southern *Pisces-Cetus* (also  $m = 9$ ). The Southern *Pisces-Cetus* is also found as SSCC 417, with  $m = 14$ . It was studied previously by Porter & Raychaudhury (2005) and Porter & Raychaudhury (2007).

**Horologium-Reticulum (SCL 048):** Studied by Fleenor et al. (2006), *Horologium-Reticulum* is MSCC 117, the second richest in MSCC. Figure 5 shows the distribution of its member clusters in 3-D. This supercluster appears significantly fragmented in SSCC, namely as SSCC 110, 117, and 122. This fragmentation is due to the smaller value of  $\ell_c$  in the southern PF ( $\sim 15 h_{70}^{-1}$  Mpc) compared to the master PF ( $\sim 22 h_{70}^{-1}$  Mpc) at  $z \sim 0.06$  (cf. Fig. 3).

**Ursa Major (SCL 109):** Is a northern supercluster listed as MSCC 310. We found good agreement between the member clusters as listed in MSCC and those listed by Kopylova & Kopylov (2009).

**Shapley (SCL 124):** Is usually described (e.g. Bardelli et al. 1994; Proust et al. 2006) as composed of three concentrations, where the central concentration is the classical Shapley supercluster (integrated by A3556, A3558, A3560, A3564, and A3566, according to Bardelli et al. 1994). This concentration was recognized by us as MSCC 389 and SSCC 261. A second concentration, composed of A3528, A3530, and A3532, is part of MSCC 389 and SSCC 249. The third condensation, called the “Front Eastern Wall”, with A3571, A3572, and A3575 as main clusters, was found by us as MSCC 401 (which contains other 7 clusters) and SSCC 267 (with other 5 clusters).

**Boötes (SCL 138):** Identified as MSCC 414. In a recent analysis of superclusters in the SDSS region (using the member galaxies instead of the member clusters), Einasto et al. (2011a) separated it into two superclusters (SCL 349 and SCL 351 according to their catalogue). These superclusters were joined by us into MSCC 414.

**Corona Borealis (SCL 158):** Is identified as MSCC 463. A recent analysis of *Corona Borealis* by Pearson et al. (2014) suggests that many of the member clusters of MSCC 463 (namely A2056, A2061, A2065, A2067, A2089, and possibly A2092) form the only system, apart from the core of Shapley (MSCC 389 and SSCC 261), that shows conclusive evidence to be a bound supercluster.

**SSCC 82:** Is the richest supercluster in the SSCC, with  $m = 38$ . This supercluster appears in MSCC as three subsystems, namely MSCC 67 (A0210, A0214A, A2895, A2927B, and A2928C), MSCC 68 (A2923D, A2926B, A2927A, A2928B, A2931A, and A2932B), and MSCC 84 with the remaining A-clusters of SSCC 82. These three su-

perclusters are connected through member clusters S0193 and S0227A in the SSCC. Einasto et al. (2001) included a fraction (nine clusters) of the clusters of SSCC 82 in SCL 232c.

**Aquarius A (SCL 205):** MSCC 576 is known as *Aquarius A* (Tully et al. 1992), or simply *Aquarius* (Einasto et al. 2001). It corresponds to SSCC 402 and has the same member clusters in both MSCC and SSCC. This membership is also in accordance with the identification of members made by Caretta et al. (2002).

**Aquarius B (SCL 209):** MSCC 574 is known as *Aquarius B* (Tully et al. 1992). It is the richest system in the MSCC, with  $m = 42$ . Batuski et al. (1999) analysed the region of this supercluster, based only on A-clusters, and suggested it to be “the largest supercluster in the Local Universe” (in fact even connected to *Aquarius A*). In our analysis it was separated into SSCC 401 ( $m = 20$ ) and SSCC 396 ( $m = 14$ ), with only a small aggregation of S-clusters to the systems. This separation is consistent with the study of Caretta et al. (2002), who considered both A- and S-clusters, also including poor clusters from other catalogs (namely APMCC, Dalton et al. 1997, and EDCC, Lumsden et al. 1992) and groups, and found that *Aquarius B* is composed of two structures with only a low probability to be connected: a wall-like structure and a filament roughly along the line of sight towards higher redshift. Thus, the inclusion of S-clusters in our sample, the SSCC, reproduces this last result, as can be seen in the 3-D map of the member clusters of *Aquarius B* in both MSCC and SSCC (Figure 6).

**Sloan Great Wall:** Another important structure is the Sloan Great Wall (Gott et al. 2005). Einasto et al. (2011b) found this structure to be integrated by the *Sextans* supercluster (SCL 88), *Leo-Sextans supercluster* (SCL 91), *Virgo-Coma* supercluster (SCL 111), and SCL 126. We found the *Sextans* supercluster as MSCC 225, while in our catalogue *Leo-Sextans* is fragmented into MSCC 247 and 273, and *Virgo-Coma* into MSCC 311, 327, 343, and 352. SCL 126 was found by us as MSCC 376.

There are other 5 MSCC objects with  $m \geq 14$  that were not the subject of individual studies: MSCC 73 (SCL 229), MSCC 76 (SCL 231), MSCC 84 and 94 (SCL 232c), and MSCC 123 (SCL 53, also known as *Fornax-Eridanus* supercluster). MSCC 238 has a multiplicity  $m = 21$ , and its member clusters are line-of-sight components of clusters in SCL 256c, but they are not dominant components (they do not have significantly high fractions of galaxies with measured redshift along the respective observing cone), except for A1028A. Another supercluster, MSCC 248, has



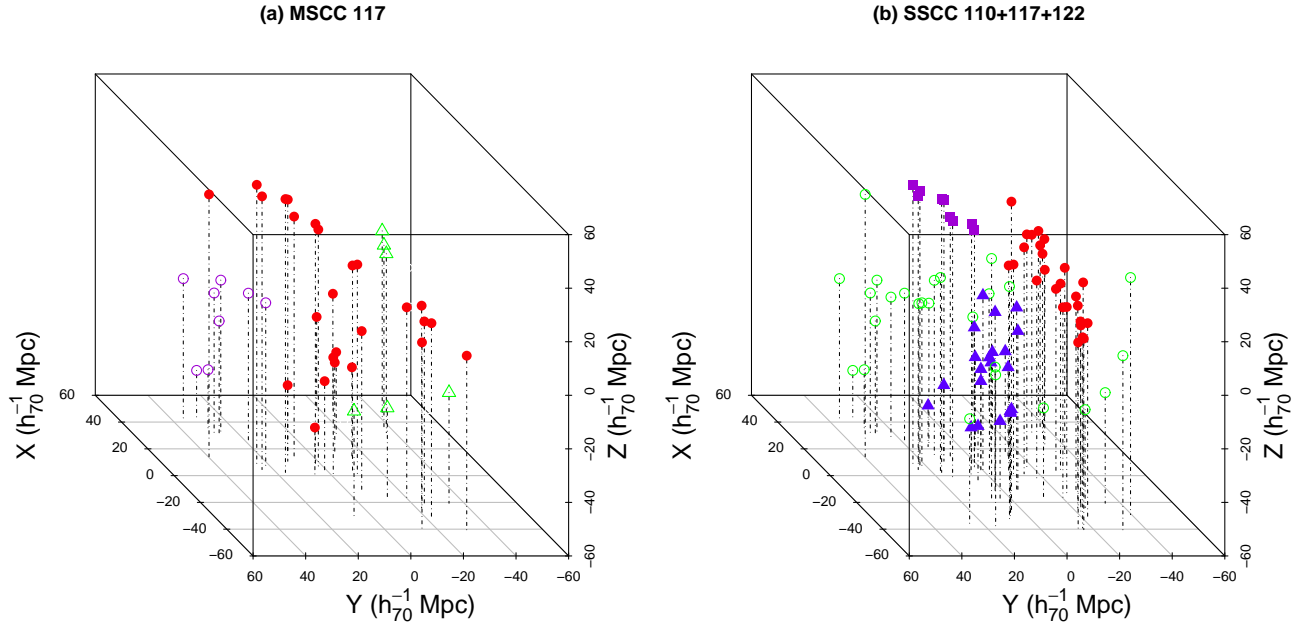


**Figure 5.** *Horologium-Reticulum* supercluster. The XYZ coordinates are derived from RA, DEC, and  $z$  of the individual clusters, where X is pointing toward RA=DEC=0, and Z=0 is pointing to the north celestial pole. Left panel: distribution of clusters in the *Horologium-Reticulum* region according to the MSCC: solid circles are members of *Horologium-Reticulum* supercluster (MSCC 117); open circles are member clusters of MSCC 115, a foreground supercluster to *Horologium-Reticulum*; and open triangles are other clusters in the volume. Right panel: distribution according to SSCC; *Horologium-Reticulum* is fragmented into three superclusters: SSCC 110 (solid circles), SSCC 117 (solid triangles) and SSCC 122 (solid squares); open circles are other clusters in the volume.

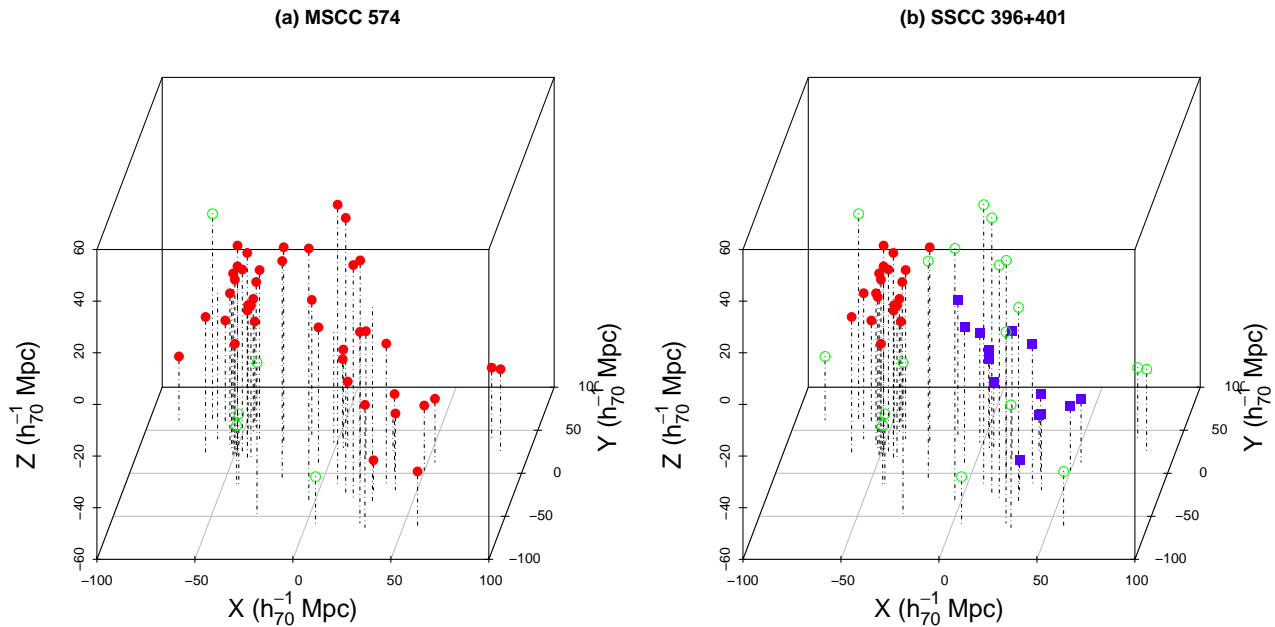


**Figure 6.** *Aquarius B* supercluster. XYZ coordinates as in Figure 5. Left panel: distribution of clusters in *Aquarius B* according to MSCC: solid circles are members of *Aquarius B*; open circles are other clusters in the considered volume. Right panel: distribution according to the SSCC; *Aquarius B* is fragmented into two superclusters: solid circles are clusters in SSCC 401, taken as the main condensation of *Aquarius B*; solid squares are members of SSCC 396, a filamentary structure toward higher redshifts; open circles are other clusters in the considered volume.

most of the dominant components of members of SCL 256c and was identified as its equivalent. Another 3 superclusters with  $m \geq 14$  in SSCC have not been studied in particular: SSCC 56 (SCL 22), SSCC 87 (SCL 232c), and SSCC 300 (MSCC 505 with  $m=13$ ; SCL 174, also known as *Microscopium* supercluster).

## 5 PROPERTIES OF THE SUPERCLUSTERS

### 5.1 The effect of the inclusion of S-clusters

A comparison of the MSCC and SSCC catalogues should give us hints on how the inclusion of S-clusters affects our description of the nearby large-scale structure. We cross-matched them to identify A-clusters in both catalogues, in order to see how the S-clusters affected their supercluster hosts. The MSCC includes 211 (35%) superclusters with  $\delta \leq -17^\circ$ . Using the sample of A-clusters with  $\delta < -17^\circ$ , we found that only 132 (62%) of these 211 have an unambiguous match with only one supercluster in SSCC (the member clusters of one MSCC supercluster were distributed in only one SSCC object). Another 29 (14%) superclusters appear divided in two or more parts in SSCC, which is likely a consequence of the fact that the critical linking length,  $\ell_c$ , is smaller for the southern sample than for the Master PF. These fragments are not necessarily less rich than their MSCC counterparts, and often the inclusion of S-clusters as members maintains their multiplicities almost equal, but their physical sizes are usually smaller, as pointed out in Section 3. This “fragmentation” is more dramatic in the richest superclusters ( $m > 15$ ). As an example, in section 4.3 we observed a certain degree of fragmentation in the richest structures such as *Aquarius B* and *Horologium-Reticulum*, into more compact or filamentary structures. Another 50 (24%) MSCC superclusters disappeared in SSCC because their member clusters were not connected by the smaller linking length. Forty-seven A-clusters, members of some supercluster in MSCC, are only accompanied by S-clusters in SSCC. We shall refer to this effect as “nucleation”.

We found that 290 isolated A-clusters of MSCC are also isolated in SSCC. Another 91 A-clusters that are isolated in MSCC became members of superclusters in SSCC. Of the total number of 423 superclusters in SSCC, 194 are considered new superclusters, i.e. they do not have an unambiguous counterpart in MSCC nor do they arise from fragmentation. Of these, 83 (42%) represent nucleation of isolated clusters in MSCC, 3 (2%) are bridges of S-clusters, i.e., isolated clusters in MSCC connected by S-clusters in SSCC, and 108 (56%) are new superclusters formed by only S-clusters (including cluster pairs with  $m = 2$ ).

Although the SSCC covers only about 35% of the whole sky (excluding the Galactic plane,  $|b| \lesssim 10^\circ$ ) the number of superclusters is about twice that in the MSCC in the same volume. As explained before, the main contributions to this enhancement of the number of superclusters are: nucleation (50%, considering both, nucleation of disconnected A-clusters being members of MSCC superclusters, as well as nucleation of isolated A-clusters in the south), S-cluster systems (40%), fragmentations (8%), and S-cluster bridges (2%).

If S-clusters are poorer systems, it may be expected

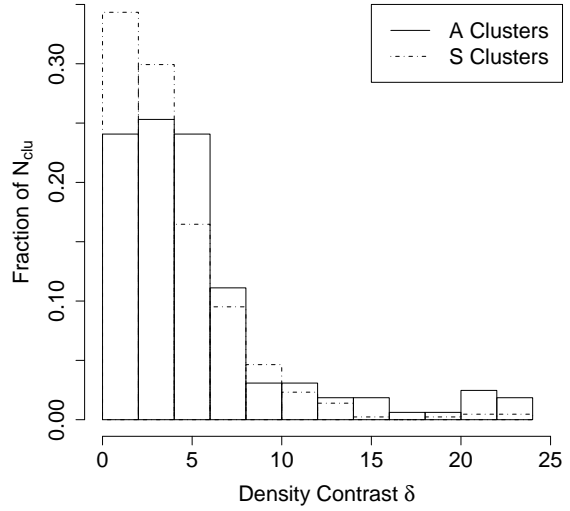


**Figure 7.** Distribution of ambient density for Abell/ACO clusters (isolated+supercluster members) in the southern sky ( $\delta < -17^\circ$ ) for  $z \leq 0.06$ , where the sample is reasonably complete for less massive systems. The density contrast is defined as the density we obtained for counting the number of any A- or S- cluster within a distance of  $20 h_{70}^{-1}$  Mpc (the mean distance between clusters) around all clusters (including the cluster itself) divided by  $2.8 \times 10^{-5} h_{70}^3 \text{ Mpc}^{-3}$  (the mean cluster density of the sample up to this redshift). Solid histogram: distribution for A-clusters. Dashed histogram: distribution for S-clusters.

**Table 5.** Statistical tests for density distributions between A and S clusters showed in Figure 7.

Test	p-value
KS	0.01
Cramér	<0.01
Tukey	<0.01

that they inhabit lower-density regions. To test this hypothesis, we determined the local number density of A- and S-clusters within  $20 h_{70}^{-1}$  Mpc for each cluster in the southern sky ( $\delta < -17^\circ$ ) with redshift  $z \leq 0.06$ . Out to this redshift, based on an examination of Figure 1, the sample seems to be reasonably complete. Figure 7 shows the histograms for the local density of southern clusters. It is apparent that S-clusters tend to inhabit lower-density regions than A-clusters. Three statistical tests were applied to corroborate this visual inspection, the Kolmogorov-Smirnov (KS), Cramér and Tukey tests. The p-values are listed in Table 5, and suggest a low probability that both distribution are drawn from the same population. This is in agreement with the scenario where the main effect of S-cluster is the nucleation, the fact that A-clusters are surrounded by S-clusters in the external regions of superclusters, or in filaments, where the density is lower.

On the other hand, we did find 108 superclusters formed only by S-clusters, but none of those has  $m > 4$ , and indeed 71% of these are pairs ( $m = 2$ ).

## 5.2 Multiplicity Functions

The multiplicity function (MF) is the distribution of multiplicities (the amount of member clusters) of the superclusters. The cumulative MFs of MSCC and SSCC catalogues are shown in Figures 8a and 8b. Both follow very closely a power law, for which we obtained the slope,  $\alpha$ , defined as  $N(> m) \propto m^\alpha$ , whose values are listed in each panel of that figure. We compared the MF obtained for MSCC and SSCC with the ones obtained for two other observational samples, as well as for two mock catalogues. We also compared them to one generated from a completely random sample.

The two other observational samples are the supercluster catalogue of Einasto et al. (2001), the equivalent all-sky supercluster catalogue based on Abell/ACO clusters before our MSCC (Figure 8c), and the catalogue of 2MASS groups (Figure 8d, Crook et al. 2007), to which we applied our FoF algorithm to create a comparison supercluster catalogue including lower mass systems. Einasto et al. (2001) show the MF for SCL, but these authors did not attempt a cumulative log-log plot of the multiplicity function which would show a power-law distribution. The SCL superclusters also follow a power law, though with a slightly higher dispersion than our MSCC and SSCC catalogues. The MFs of the three supercluster samples (MSCC, SSCC, and SCL) have similar slopes:  $\alpha \sim -1.9$ . Figure 8d shows the MF for a supercluster catalogue based on 2MASS “groups” (Crook et al. 2007), which dominantly consists of systems of lower mass than the S-clusters in SSCC, but includes the few rich Abell clusters that exist within its redshift limit ( $z_{lim} \sim 0.033$ ). This catalogue, only produced to check the presence of a power law in its MF, was obtained using a PF similar to the ones generated for MSCC and SSCC in order to compensate for the selection effects with the redshift. The power law seems to apply to systems of very different mass, and, since the SCL was produced using a single critical linking length,  $\ell_c$ , for the entire volume, it also seems to be independent of the selection of  $\ell_c$  to produce the catalogue.

Can the mock catalogues based on simulated data reproduce the MFs of the observational samples? The distribution generated from mock catalogues come from the Millennium simulation (Figure 8e, Springel et al. 2005) and Bolshoi simulation (Figure 8d, Klypin et al. 2011).

The Millennium project is a  $\Lambda$ CDM N-body simulation of the evolution, since redshift  $z=127$ , of  $2160^3$  (cold dark matter) particles within a box of side 500 Mpc based on  $H_0 = 73 \text{ km s}^{-1} \text{ Mpc}^{-1}$ . For the FoF calculations in the present paper all cosmological parameters were scaled to  $H_0 = 70 h_{70} \text{ km s}^{-1} \text{ Mpc}^{-1}$ , thus the box side corresponds to  $521 h_{70}^{-1} \text{ Mpc}$ . The mass of the individual particles is  $M/M_\odot = 8.98 \times 10^8 h_{70}^{-1}$ . We selected all dark matter haloes obtained from the internal FoF of the Virgo-Millennium Database (<http://gavo.mpa-garching.mpg.de/Millennium/>) with the condition  $M/M_\odot \geq 10^{13} h_{70}^{-1}$  ( $\geq 11136$  particles per dark matter halo). The dark matter halo sample obtained in this way has a density of similar order as that obtained for the sample of 2MASS groups (Table 6). We applied our own FoF to the 51998 massive dark matter haloes that follow the mass condition within the complete volume of the Millennium simulation, which corresponds to a redshift limit of  $z \sim 0.12$ . Since the mean density is by construction the same throughout the Millennium volume, we assumed a constant

**Table 6.** Comparison of properties of different samples of “particles” used to study the multiplicity function. Columns are: (1) the name of the sample, (2) the number of groups/clusters/particles within the considered volume, (3) the volume in units of  $h_{70}^{-3} \text{ Gpc}^3$ , for MSCC, SSCC, SCL, and 2MASS groups, excluding the zone of avoidance near the Galactic plane, (4) the density,  $\bar{n}$ , of groups, clusters or dark matter haloes, excluding the zone of avoidance where necessary, and (5) the slope  $\alpha$  fitted to the cumulative multiplicity function.

Catalogue based	N clu/par	Volume ( $h_{70}^{-3} \text{ Gpc}^3$ )	$\bar{n}$ ( $h_{70}^3 \text{ Mpc}^{-3}$ )	$\alpha$
MSCC	3410	$82.5 \times 10^{-2}$	$\leq 7.4 \times 10^{-6}$	-2.00
SSCC	2385	$30.5 \times 10^{-2}$	$\leq 2.8 \times 10^{-5}$	-1.91
SCL	1663	$54.5 \times 10^{-2}$	$3.0 \times 10^{-6}$	-1.87
2MASS groups	1261	$1.0 \times 10^{-2}$	$5.3 \times 10^{-4}$	-1.67
Millennium	51998	$14.2 \times 10^{-2}$	$3.5 \times 10^{-4}$	-3.09
Bolshoi	5585	$1.6 \times 10^{-2}$	$3.4 \times 10^{-4}$	-2.36
Random	7329	$99.8 \times 10^{-2}$	$7.4 \times 10^{-6}$	-3.85

value of  $\ell_c$  throughout the volume. Thus,  $\ell_c$  was obtained considering the total volume and not parts of it as MSCC and SSCC (and the sample of 2MASS group). However, it is clear from Figure 8e that the distribution of superclusters obtained from such haloes does not follow the power law obtained for observational samples.

The other mock catalogue (Figure 8f) is based on the sample of dark matter haloes of the Bolshoi simulation, a  $\Lambda$ CDM N-body simulation that uses  $2048^3$  dark matter particles within a box of side  $250 h_{70}^{-1} \text{ Mpc}$ . It has the largest resolution for a cosmological simulation of this type, not only in space but also in time evolution. For comparison, Millennium is based on 11 000 time steps per particle while Bolshoi was evolved since  $z = 80$  in  $\sim 400 000$  time steps. The simulation was obtained with the Adaptive-Mesh-Refinement (AMR)-type code (Kravtsov et al. 1997) instead of the GADGET code (Springel et al. 2001) used for Millennium. For Bolshoi, we extracted from the MultiDark Database (<http://www.multidark.org/MultiDark/>) such haloes with  $M/M_\odot \geq 10^{13} h_{70}^{-1}$  (haloes were determined by an internal FoF of the MultiDark Project). The particle density of Bolshoi is, again, comparable to that of the 2MASS group sample, and similar to the sample of massive haloes of Millennium we used (cf. Table 6). We applied our FoF to these haloes, using the same procedure as for Millennium. The MF for superclusters we obtained in this way follows more closely the power law than the mock catalogue obtained with Millennium, but yet it is evident that neither of the two mock catalogues produce a cumulative MF that resembles the power-law distribution of multiplicities for the real superclusters.

While the observational MF distributions for higher mass systems are relatively well fitted by a power law with  $\alpha \sim -2.0$ , the simulated ones do not follow closely a power law, presenting a more curved distribution (lower fraction of superclusters with low and high multiplicities, and larger for intermediate multiplicities than in a power law regime), resulting in lower values for  $\alpha$ .

What would one expect from a completely random sample of particles? Figure 8g is the average of the MF of one thousand simulated catalogues based on randomly dis-

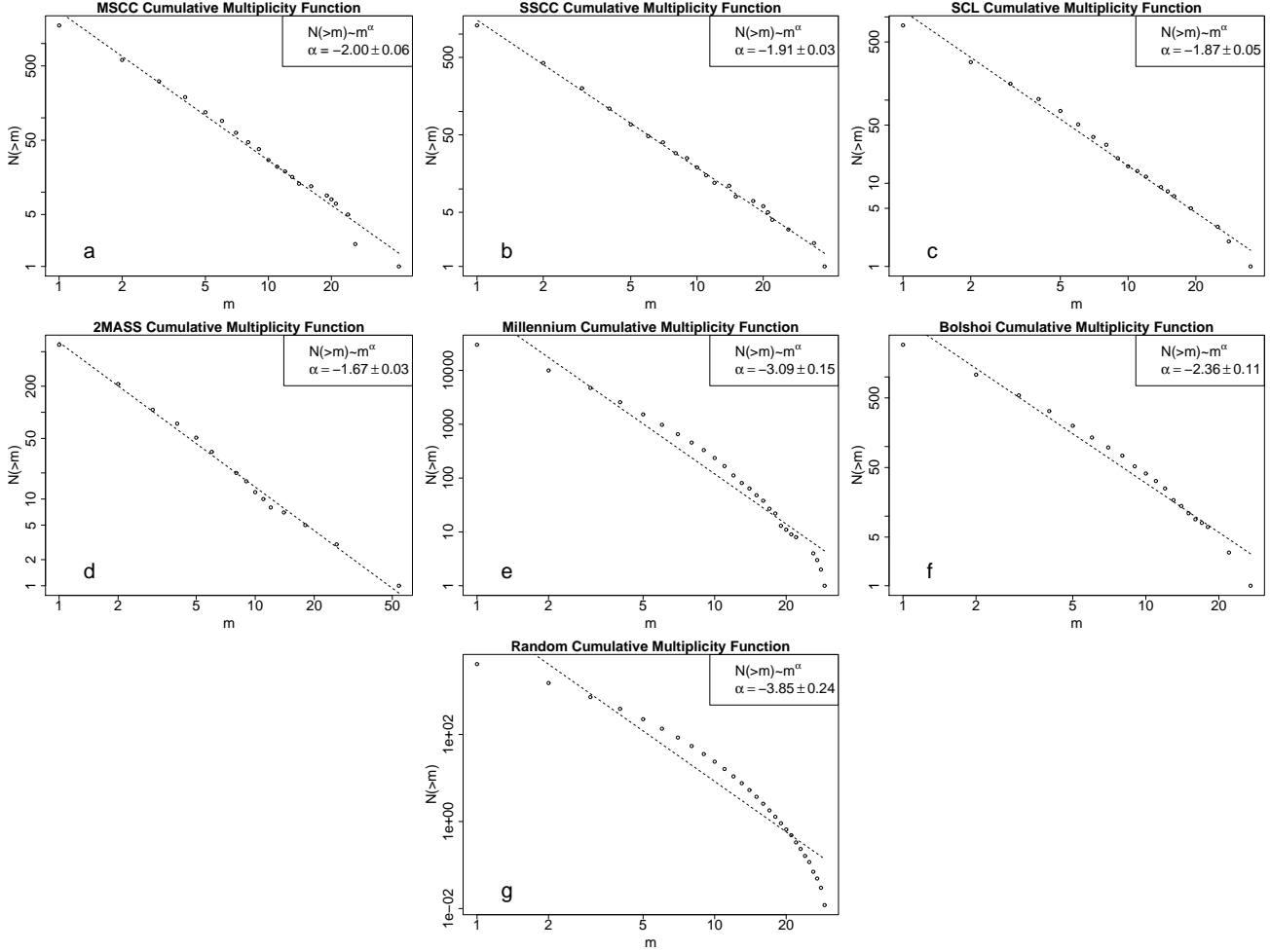


**Figure 8.** Multiplicity functions for: (a) MSCC, (b) SSCC, (c) SCL, and supercluster catalogues based (d) on 2MASS groups, (e) on a mock catalogue obtained from the Millennium simulation, (f) on a mock catalogue obtained from the BOLSHOI simulation, and (g) on the average of one thousand simulated mock catalogues of randomly distributed points with a mean density of  $\bar{n} = 7.4 \times 10^{-4} h_{70}^3 \text{ Mpc}^{-3}$  (the cluster density of the input sample for MSCC). See the text for details.

tributed points that represent Abell/ACO clusters. These distributions were produced assigning random coordinates to each point. Each distribution contains 7329 points in a spherical volume of “radius”  $z = 0.15$ . This condition simulates the mean density of the best-sampled region of MSCC. In each sample, the value of the critical linking length,  $\ell_c$ , was found, and a FoF algorithm was applied. We produced one thousand mock supercluster catalogues, from which the number of frequency of each richness was averaged (note that this resulted in high-richness systems having fractional values of frequency in Figure 8g). Again, as for the other distributions, the slope  $\alpha$  is shown, but neither the cosmological simulations nor the random distribution reproduces the shape of the cumulative multiplicity function of the observational samples. Actually, the completely random sample appears more similar to the distribution based on the Millennium data.

The hump in the curves based on mock catalogues, much stronger in the random and Millennium MF, can be interpreted as a lower probability to obtain high-richness superclusters from such samples. We can see this in the random distribution, where the structures are in a Poissonian

regime and the value of the power spectrum is expected to be zero. However, in a gravitational regime one may expect to obtain structures (power spectrum  $> 0$ ), that drive the superclusters toward the richest systems, which would explain why in the MF of cluster-based catalogues the curves do not decay (at the rich end) as abruptly as in the random case.

Power laws have also been fitted in the literature for the number of galaxies within groups of SDSS by Berling et al. (2006) and Nurmi et al. (2013). Berling et al. (2006) found values for  $\alpha$  of  $2.49 \pm 0.28$ ,  $2.48 \pm 0.14$  and  $2.72 \pm 0.16$  for different volume-limited samples of absolute magnitude limits of  $M_r \leq -18$ , and  $-19$ ,  $-20$ . On the other hand, Nurmi et al. (2013) found  $2.02 \pm 0.18$ ,  $2.12 \pm 0.17$ ,  $2.26 \pm 0.19$  for these luminosity ranges, and  $3.29 \pm 0.24$  for  $M_r \leq -21$ . Since these distributions are based on “particles” (galaxies) of much lower mass we do not expect a direct relation with those obtained here, except, as we said, that the power law will be a natural distribution for systems in gravitational regimes.

## 6 CONCLUSIONS AND SUMMARY

We summarize our conclusions as follows.

1. We constructed two new supercluster catalogues based on the optically-selected Abell/ACO clusters, which not only reach deeper in space ( $z \leq 0.15$ ) than previous ones, but also contain a much higher fraction ( $\gtrsim 85\%$ ) of clusters with spectroscopically confirmed redshifts. Different from previous works, we include in our analysis the different line-of-sight components for the clusters (up to the above-mentioned redshift limit). One of these catalogues is the all-sky Main SuperCluster Catalogue (MSCC), based on only the rich Abell A-clusters, the other is the Southern SuperCluster Catalogue (SSCC) covering declinations  $\delta < -17^\circ$  and including the supplementary Abell S-clusters.

2. A tunable linking length was used to generate these supercluster catalogues, taking into account the undersampling at higher redshift and the different selection functions in different regions of the sky. The area covered by SDSS is clearly better sampled than the rest of the sky, and a special percolation function was fitted for this region. Also, for the southern sky, the inclusion of the S-clusters required an independent correction for the selection function. We conclude that the “percolation function” is an efficient tool for detecting and correcting the selection function for samples of galaxy clusters.

3. For the all-sky main sample of A-clusters we found that the maximum completeness is reached near  $z \sim 0.06$ , which leads to a critical linking length of  $\ell_c \sim 22.5 h_{70}^{-1}$  Mpc, while for the south ( $\delta < -17^\circ$ ) the S-clusters provide the best sampling at  $z \sim 0.01$ , leading to  $\ell_c \sim 11.5 h_{70}^{-1}$  Mpc.

4. The MSCC and the SSCC contain 601 and 423 superclusters, respectively. Considering the probability for a cluster to be member of a supercluster or not, we found the following: 35% of the clusters tend to be isolated, 18% form pairs and 47% are hosted by a supercluster with  $m \geq 3$ . Of the superclusters found, the fraction of pairs ( $m = 2$ ) is  $\sim 50\%$ , while the fraction of very rich superclusters ( $m > 10$ ) is  $\sim 4\%$  of the systems. The complete catalogues and input lists of clusters are available in the electronic version of this paper.

5. By comparing our MSCC directly with the one by Einasto et al. (2001) we find: (1) a slightly higher fraction of isolated clusters (35% compared to 30% in SCL); (2) 37 new superclusters identified in the same volume investigated previously; (3) 126 new superclusters near and beyond  $z = 0.13$ ; (4) 70% of Einasto et al.’s candidate superclusters were not confirmed as such. The fraction of candidate superclusters was reduced from 40% to 6%, thanks to the much higher fraction of clusters with spectroscopically confirmed redshifts in our sample.

6. Comparison between the MSCC and SSCC reveals that the S-clusters seem to prefer to inhabit the surroundings of richest clusters. The lower critical linking length in SSCC only breaks up the MSCC systems with  $m \geq 15$  and, since these systems represent only  $\sim 2.0\%$  of the MSCC, and only 1.2% of them are in the declination range of SSCC, this fragmentations is not significant. More important effects of the inclusion of S-clusters on the distribution are new superclusters (with multiplicities  $m \geq 2$ ) of only S-clusters and the “nucleation” of A-clusters surrounded by S-clusters.

7. The distributions of supercluster “richness” (the mul-

tiplicity function) of the MSCC and SSCC follow a power law of slope  $\alpha \sim -2.0$ . A very similar behaviour is seen in other catalogues based on observational data, namely the SCL (Einasto et al. 2001) and a catalogue generated from 2MASS groups (Crook et al. 2007), the latter being far more complete for lower-mass systems. However, when similar supercluster catalogs are generated from mock data, namely using the Millennium (Springel et al. 2005) and the Bolshoi (Klypin et al. 2011) N-body cosmological simulations, the multiplicity functions change from a power law to a convex curve, predicting less superclusters in both the low- and high-multiplicity regimes. A similar behaviour, even farther from a power law, is found for an entirely random distribution of input clusters.

## ACKNOWLEDGMENTS

We thank Kristin Riebe and the people of the Multi-Dark Project as well as Gerard Lemson and the people of the Virgo Consortium for the access to the databases of the cosmological simulations used in this paper. We also thank the R Core Team (2013) and other developers of R Project libraries: Ligges & Mächler (2003), Franz (2006), Hothorn et al. (2008), Warnes et al. (2014), and Zeileis (2004). All graphics and statistics in this work were generated using these tools. M.C.-M. acknowledges a CONACyT grant for a Master thesis, and C.C. and H.A. a Guanajuato University grant #219/13. C.C. and H.A. are also grateful to the staffs of the following observatories, where some of the spectroscopic data used in this paper were obtained: Observatorio Astronómico Nacional (Ensenada, Mexico), Observatorio do Pico dos Dias (Brasópolis, Brasil), South African Astronomical Observatory (Cape Town, South Africa) and Indian Astronomical Observatory (Hanle, India).

## REFERENCES

- Abazajian, K., Adelman-McCarthy, J.K., Agüeros, M.A., et al, 2004, ApJS, 182, 543
- Abell, G.O., 1958, ApJS, 3, 211
- Abell, G.O., 1961, AJ, 66, 60
- Abell, G.O., Corwin, Jr., H.G., Olowin, R.P., 1989, ApJS, 70, 1
- Andernach, H., 1991, in *Large-Scale Structures and Peculiar Motions*, eds. D.W. Latham & L.N. da-Costa), ASP. Conf. Ser. 15, 279
- Andernach, H., Tago, E., 1998, in “Large Scale Structure: Tracks and Traces”, eds. V. Müller, S. Gottlöber, J.P. Mückel, J. Wambsgans, p. 147, Singapore: World Scientific
- Andernach, H., Tago, E., Einasto, J., Stengler-Larrea, E., 1995, ApL&C, 31, 27
- Andernach, H., Tago, E., Einasto, M., Einasto, J., Jaaniste, J., 2005, ASPC, 329, 283
- Bahcall, N. A., Soneira, R. M., 1984, ApJ, 277, 27
- Bardelli, S., Zucca, E., Vettolani, G., Zamorani, G., Scaramella, R., Collins, C.A., MacGillivray, H.T., 1994, MNRAS, 267, 665
- Barmby, P., Huchra, J.P., 1998, AJ, 116, 1508

- Batuski, D.J., Miller, C.J., Slingsend, K.A., 1999, *AJ*, 520, 491
- Batuski, D.J., Burns, J.O., 1985, *AJ*, 90, 1413
- Beers, T. C., Forman, W., Huchra, J. P., Jones, C., & Gebhardt, G., 1991, *AJ*, 102, 1581
- Berlind, A.A., Frieman, J., Weinberg, D.H., Blanton, M.R., Warren, M.S., Abazajian, K., Scranton, R., Hogg, D.W., Scoccamarro, R., Bahcall, N.A., Brinkmann, J., Gott, III, J.R., Kleinman, S.J., Krzesinski, J., Lee, B.C., Miller, C.J., Nitta, A., Schneider, D.P., Tucker, D.L., Zehavi, I., SDSS Collaboration, 2006, *ApJS*, 167, 1
- Bogart, R.S., Wagoner, R.V., 1973, *ApJ*, 181, 609
- Caretta, C.A., Maia, M.A.G., Kawasaki, W., Willmer, C.N.A., 2002, *AJ*, 123, 1200
- Caretta, C.A., Rosa, R.R., Campos Velho, H.F., Ramos, F.M., Makler, M., 2008, *A&A*, 487, 445
- Chon, G., Böhringer, H., Nowak, N., 2013, *MNRAS*, 429, 3272
- Colless, M., Dalton, G., Maddox, S., et al., 2001, *MNRAS*, 1039, 1063
- Costa-Duarte, M.V., Sodr e, L., Jr., Durret, F., 2011, *MNRAS*, 411, 1716
- Crook, A.C., Huchra, J.P., Martimbeau, N., Masters, K.L., Jarrett, T., Macri, L.M., 2007, *ApJ*, 655, 790
- Dalton, G.B., Maddox, S.J., Sutherland, W.J., Efstathiou, G., 1997, *MNRAS*, 289, 263
- de Vaucouleurs, G., 1953, *AJ*, 58, 30
- Einasto, J., Klypin, A.A., Saar, E., Shandarin, S.F., 1984, *MNRAS*, 206, 529
- Einasto, M., Einasto, J., Tago, E., Dalton, G.B., Andernach, H., 1994, *MNRAS*, 269, 301
- Einasto, M., Tago, E., Jaaniste, J., Einasto, J., Andernach, H., 1997, *A&AS*, 123, 119
- Einasto, M., Einasto, J., Tago, E., M uller, V., Andernach, H., 2001, *AJ*, 122, 2222
- Einasto, J., Einasto, M., Tago, E., Saar, E., H utsi, G., J oeveer, M., Liivam agi, L.J., Suhhonenko, I., Jaaniste, J., Hein am aki, P., M uller, V. and Knebe, A. and Tucker, D., 2007a, *A&A*, 462, 811
- Einasto, J., Einasto, M., Saar, E., Tago, E., Liivam agi, L.J., J oeveer, M., Suhhonenko, I., H utsi, G., Jaaniste, J., Hein am aki, P., M uller, V., Knebe, A., Tucker, D., 2007b, *A&A*, 462, 397
- Einasto, M., Einasto, J., Tago, E., Liivam agi, L.J., J oeveer, M., H utsi, G., Hein am aki, P., M uller, V., Tucker, D., 2007c, *A&A*, 464, 815
- Einasto, M., Saar, E., Liivam agi, L.J., Einasto, J., Tago, E., Mart inez V.J., Starck, J.L., M uller, V., Hein am aki, P., Nurmi, P., Gramann, M., H utsi, G., 2007d, *A&A*, 476, 697
- Einasto, M., Liivam agi, L.J., Saar, E., Einasto, J., Tempel, E., Tago, E., Mart inez, V.J., 2011a, *A&A*, 535, 36
- Einasto, M., Liivam agi, L.J., Tempel, E., Saar, E., Tago, E., Einasto, P., Enkvist, I., Einasto, J., Mart inez, V.J., Hein am aki, P., Nurmi, P., 2011b, *ApJ*, 736, 51
- Fleener, M.C., Rose, J.A., Christiansen, W.A., Johnston-Hollitt, M., Hunstead, R.W., Drinkwater, M.J., Saunders, W., 2006, *AJ*, 131, 1280
- Franz, C. (2006). cramer: Multivariate nonparametric Cramer-Test for the two-sample-problem. R package version 0.8-1. <http://CRAN.R-project.org/package=cramer>
- Giovannelli, R., Haynes, M.P., 1993, *AJ*, 105, 1251
- Gott III, J.R., Juri c, M., Schlegel, D., Hoyle, F., Vogeley, M., Tegmark, M., Bahcall, N., Brinkmann, J., 2005, *ApJ*, 624, 463
- Gramann, M., Suhhonenko, I., 2002, *MNRAS*, 337, 1417
- Gregory, S.A., Thompson, L.A., 1978, *ApJ*, 222, 784
- Hauser, M.G., Peebles, P.J.E., 1973, *ApJ*, 185, 757
- Hanski, M.O., Theureau, G., Ekholm, T., Teerikorpi, P., 2001, *A&A*, 378, 345
- Hogg, D.W., 2000, [arXiv:astro-ph, 9905116v4](http://arxiv.org/abs/astro-ph/9905116v4)
- Hothorn, T., Bretz, F., Westfall, 2008, *Biometrical Journal* 50(3), 346, 363
- Huchra, J.P., Geller, M.J., 1982, *ApJ*, 257, 4237
- Jaaniste, J., Tago, E., Einasto, M., Einasto, J., Andernach, H., M uller, V., 1998, *A&A*, 336, 35
- Jones, H., Saunders, W., Colless, M., et al. 2004, *MNRAS*, 355, 747
- Kalinkov, M., Kuneva, I., 1995, *A&AS*, 113, 451
- Klypin, A.A., Trujillo-Gomez, S., Primack, J., 2011, *ApJ*, 740, 102
- Kolokotronis, V., Basilakos, S., Plionis, M., 2002, *MNRAS*, 331, 1020
- Kopylova, F., Kopylov, A., 2009, *AstBu*, 64, 1
- Kravtsov, A.V., Klypin, A.A., Khokhlov, A.M., 1997, *ApJS*, 111, 73
- Ligges, U., M achler, M. (2003). Scatterplot3d - an R Package for Visualizing Multivariate Data. *Journal of Statistical Software* 8(11), 1-20.
- Lumsden, S.L., Nichol, R.C., Collins, C.A., Guzzo, L., 1992, *MNRAS*, 258, 1
- Luparello, H., Lares, M., Lambas, D.G., Padilla, N., 2011, *MNRAS*, 415, 964
- Lynden-Bell, D., Faber, S.M., Burstein, D., Davies, R.L., Dressler, A., Terlevich, R.J., Wegner, G., 1988, *ApJ*, 326, 19
- Nurmi, P., Hein am aki, P., Sepp, T., Tago, E., Saar, E., Gramann, M., Einasto, M., Tempel, E., Einasto, J., 2013, 436, 380,
- Obayashi, H., Makishima, K., Tamura, T., 1998, *PASJ*, 50, 573
- Oort, J.H., 1983, *ARA&A*, 21, 373
- Peacock, J.A., West, M.J., 1992, *MNRAS*, 259, 494
- Peebles, P.J.E., 1974, *Ap&SS*, 31, 403
- Pearson, D.W., Batiste, M., Batuski, D.J., 2014, *MNRAS*, 441, 1601
- Planck Collaboration: Ade, P.A.R., et al., 2013, *A&A*, 550A, 134
- Porter, S.C., Raychaudhury, S., 2005, *MNRAS*, 364, 1387
- Porter, S.C., Raychaudhury, S., 2007, *MNRAS*, 375, 1409
- Proust, D., Quintana, H., Carrasco, E.R., Reisenegger, A., Slezak, E., Muriel, H., D unner, R., Sodr e Jr., L., Drinkwater, M.J., Parker, Q.A., Ragone, C.J., 2006, *A&A*, 477, 133
- Quintana, H., Ramirez, A., Melnick, J., Raychaudhury, S., Slezak, E., 1995, *AJ*, 110, 463
- R Core Team. R: A language and environment for statistical computing. R Foundation for Statistical Computing, Vienna, Austria. URL <http://www.R-project.org/>
- Rood, H.J., 1976, *ApJ*, 207, 16
- Sato, K., Kelley, R., Takei, Y., Tamura, T., Yamasaki, N.Y., Ohashi, T., Gupta, A., Galeazzi, M., 2010, *PASJ*, 62, 1445
- Sousbie, T., 2011, *MNRAS*, 414, 350

- Sousbie, T., Pichon, C., Kawahara, H., 2011, MNRAS, 414, 384
- Springel, V., Yoshida, N., White, Simon D.M., 2001, NewA, 6, 79
- Springel, V., White, S.D.M., Jenkins, A., Frenk, C.S., Yoshida, N., Gao, L., Navarro, J., Thacker, R., Croton, D., Helly, J., Peacock, J.A., Cole, S., Thomas, P., Couchman, H., Evrard, A., Colberg, J., Pearce, F., 2005, Natur, 435, 629
- Thuan, T.X., 1980, in “Physical Cosmology”, Proc. Les Houches Summer School, July 1979, Amsterdam, North-Holland Publ., p. 277
- Tully, R.B., Scaramella, R., Vettolani, G., Zamorani, G., 1992, ApJ, 388, 9
- Turner, E.L., Gott, III, J.R., 1976, ApJS, 32, 409
- Voges, W., et al., 1999, A&A, 349, 389
- Warnes, G.R., Bolker, B., Bonebakker, L., Gentleman, R., Liaw, W.H.A., Lumley, T., Maechler, M., Magnusson, A., Moeller, S., Schwartz, M., Venables, B. (2014). *gplots: Various R programming tools for plotting data.* R package version 2.13.0. <http://CRAN.R-project.org/package=gplots>
- West, M.J., 1989, ApJ, 347, 610
- Wray, J.J., Bahcall, N.A., Bode, P., Boettiger, C., Hopkins, P.F., 2006, ApJ, 652, 907
- Zeldovich, Y.B., Einasto, J., Shandarin, S.F., 1982, Nature 300, 407
- Zeileis, A. (2004). *Econometric Computing with HC and HAC Covariance Matrix Estimators.* Journal of Statistical Software 11(10), 1-17. URL <http://www.jstatsoft.org/v11/i10/>.
- Zucca, E., Zamorani, G., Scaramella, R., Vettolani, G., 1993, ApJ, 407, 470